



Ball milling synthesis of covalent organic framework as a highly active photocatalyst for degradation of organic contaminants

Hongzhou Lv^{a,b,c}, Xiaoli Zhao^{a,*}, Hongyun Niu^b, Sijing He^b, Zhi Tang^a, Fengchang Wu^a, John P. Giesy^d

^a State Key Laboratory of Environmental Criteria and Risk Assessment, Chinese Research Academy of Environmental Sciences, Beijing 100012, China

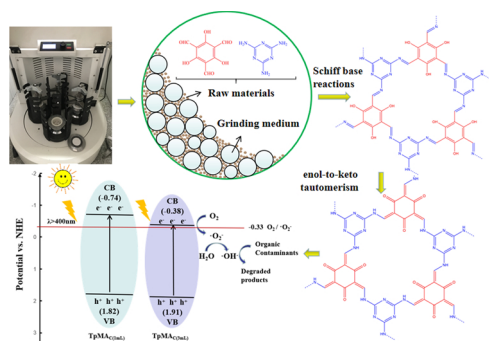
^b State Key Laboratory of Environmental Chemistry and Ecotoxicology, Research Center for Eco-Environmental Sciences, Chinese Academy of Sciences, Beijing 100085, China

^c College of Environment, Hohai University, Nanjing 210098, China

^d Department of Veterinary Biomedical Sciences and Toxicology Centre, University of Saskatchewan, Saskatoon, Saskatchewan, Canada



GRAPHICAL ABSTRACT



ARTICLE INFO

Keywords:

Covalent organic framework
Mechanochemical fabrication
Ball milling
TpMA
Photocatalysis

ABSTRACT

Facile, environmentally-friendly fabrication of high-yield and stable covalent organic framework (COF) materials has been a limitation to their large-scale production and application. In this work, ball milling was used to synthesize COF by mechanochemical reaction between 1,3,5-triformylphloroglucinol (Tp) and melamine (MA) at ambient temperature. Different routes (liquid-free, solvent-assisted and catalyst-assisted) and proportions of liquids (solvents or catalyst) were investigated. Two morphologies were obtained when various amounts of liquid were added during grinding. The two forms were interwoven thread-shaped and exfoliative thin ribbon-like structures. Further, visible-light photocatalytic ($\lambda > 400 \text{ nm}$) performance and mechanism of the two structures of COFs were investigated. The exfoliative ribbon-like structures exhibited greater rates of photodegradation of phenol and retained 87.6% of initial photodegradation after being used four times. Addition of liquid catalyst not only improved crystallinity of the COF materials, but also enhanced rates of photocatalytic reactions. Photocatalytic activity of the exfoliative structure of TpMA synthesized by ball milling was comparable with that of the photocatalyst prepared by use of the solvothermal method, while time to prepare the catalyst was shortened by 36-fold and the amount of solvent used was reduced by 8-fold at room temperature. Mechanochemical synthesis is a promising potential tool for large-scale production of COFs, which will make greater use of COFs for degradation of pollutants.

* Corresponding author.

E-mail address: zhaoxiaoli_zxl@126.com (X. Zhao).

<https://doi.org/10.1016/j.jhazmat.2019.02.046>

Received 18 December 2018; Received in revised form 9 February 2019; Accepted 12 February 2019

Available online 13 February 2019

0304-3894/ © 2019 Elsevier B.V. All rights reserved.

1. Introduction

A wide variety of materials, including porous metal organic frameworks (MOFs) [1–3], graphitic carbon nitride nanosheets (CNNs) [4,5] and covalent organic frameworks (COFs), have been fabricated to remove environmental pollutants. Compared with MOFs, COFs are a class of crystalline porous polymers consisting of highly ordered, organic building blocks [6,7], which have advantages such as low density, adjustable pore size and metal-free structure [8–11]. Meanwhile, due to their potential applications in the fields of gas storage [12,13], separation [14,15], catalysis [16,17], optoelectronic devices [18] and others [19,20], COFs have recently been studied widely.

The most extensively used method for production of COFs is solvothermal synthesis, which mainly includes mixing monomers with relatively large quantities of solvents into a sealed reactor, under certain pressure and temperature, which facilitates interactions among precursors, such that after 72–90 h, thermodynamically stable crystalline products are obtained [21]. Harsh experimental conditions of the solvothermal process, such as reaction times of several days and heating at usually 120 °C have limited large-scale production, and the crystallinity of produced polymers is influenced by combinations of solvents and their ratios during synthesis [22]. Solubility and boiling points of monomers in solvents sometimes limit solution-based syntheses of COFs [23]. Moreover, toxic potencies and costs of solvents have also made synthesis of COF challenging.

Rapid, easy and more environmentally friendly systems for synthesis of porous COFs are desirable, especially on an industrial scale. Mechanochemical synthesis, although an old technology, might be a novel method for large-scale production of COFs [24]. During the ball milling procedure, solid raw materials are caught between dynamic impacting balls, such that sizes of particles are decreased, shapes are changed, chemical bonding is broken and new surfaces are gradually produced at room temperature by kinetic energies of the balls [25,26]. In comparison with solvothermal synthesis, ball milling is potentially a scalable, energy-efficient, low-cost method of producing COFs, meanwhile, reducing amounts of solvents used or even avoiding use of solvents make it an widely required method.

Recent advances have suggested this method as a powerful tool for use in materials science, such as for fabricating zeolites [27] and metal-organic frameworks (MOFs) [28,29]. However, few methods of production of COFs have utilized grinding, particularly those based on Schiff reactions. Ball milling is still a relatively new method for synthesis of COFs and it is limited by heterogeneities of products, moderate porosity and limited crystallinity [30]. Thus, it was deemed that more work was needed to not only overcome these limitations, but also to modify ball milling approaches, which can enhance practicality of mechano-chemically synthesized COFs.

Melamine is a relatively abundant and inexpensive triazine monomer. The nitrogen (N) accounts for 66% of the mass of melamine, while the s-triazine ring provides stability, such that melamine is an excellent material for fabrication of polymers [31,32]. A highly stable, novel TpMA COF synthesized by use of a solvothermal process, has recently been shown to have superior photocatalytic capacity for degradation of phenol and methyl orange, than graphitic carbon nitride (g-C₃N₄) [33]. TpMA was synthesized by use of a modified Schiff base reaction between 1,3,5-triformylphloroglucinol (Tp) and melamine (MA), where the enol-keto tautomerism gave the framework remarkable stability toward water, acid, and base.

In the present work, a rapid, one-step ball milling method was developed to bottom-up synthesize TpMA by co-grinding of Tp and MA. Synthesis of COF (TpMA) with predetermined topological design was demonstrated by use of appropriate symmetry combinations (C₃ + C₃) of building blocks. In order to optimize reaction conditions, solvent-assisted, catalyst-assisted and liquid-free ball milling route with various liquid additions were employed. Optimal reaction conditions were determined, which provided high yields of powder of homogeneous

morphology. To examine the feasibility of this photocatalyst, phenol and methyl orange dye were selected as model compounds and mechanisms of photocatalytic degradation were elucidated.

2. Experimental

2.1. Materials

All chemicals were used without further purification. 1,3,5-triformylphloroglucinol (TP) was purchased from Toronto Research Chemicals Inc. (Toronto, Canada). Melamine (MA), *p*-toluenesulfonic acid (PTSA), 1,4-dioxane, mesitylene, *N,N*-dimethylformamide (DMF), dimethyl sulfoxide (DMSO), tert-butanol, and *p*-benzoquinone were purchased from J&K Chemical Co. Ltd. (Beijing, China). Glacial acetic acid, acetone, phenol, methyl orange, ethylenediaminetetraacetic acid disodium salt (EDTA-2Na) were obtained from Sinopharm Chemistry Reagent Co. Ltd. (Beijing, China). Ultrapure water was produced by a Milli-Q Advantage A10 water purification system (Millipore, Bedford, MA, USA).

2.2. Preparation of TpMA

Ball milling synthesis was conducted to produce TpMA by use of a planetary ball mill (model: Grinder BM4) that generated dynamic energies by differences in speeds between balls and grinding jars. 1,3,5-triformylphloroglucinol (Tp: 0.9 mmol, 189 mg) and melamine (MA: 1.35 mmol, 170 mg) were placed in a 50 mL zirconia grinding jar, with fifteen 7 mm diameter and five 5 mm diameter zirconia balls. Then the tests were conducted under different liquids (Table 1).

In liquid-free method, the mixture was ground directly at room temperature and at a rotational speed of 300 rpm for 3 h, other tests were conducted at this combination of temperature and speed. In solvent-assisted route, before grinding, solutions (a, b and c in Table 1) were added separately into the reactor. These three solvents are commonly used in syntheses of porous polymeric materials, and two addition amounts of the solution (3 or 1 mL) were investigated; In the catalyst-assisted method, different with formers, 3 or 1 mL *p*-toluenesulfonic acid catalyst were added to grinding jars followed by addition 1.35 mmol melamine. The mixture was ground first for 15 min, then 0.9 mmol TP was added to the mixture and grind was continued for 2.5 h, then 3–5 drops of water were added to the mixture and it was ground again for another 15 min. Next, the sample container was filled with water for washing off the Catalyst (PTSA).

To remove residual unreacted reactants, produced materials were sequentially treated 3–6 times with *N,N*-Dimethylformamide, acetone and ultrapure water then dried under reduced pressure at 80 °C. The yield (mass ratio of raw materials to product) was about 85%.

2.3. Photo-catalysis

Representative, organic contaminants phenol and methyl orange dye were chosen to evaluate the visible light catalytic activity of TpMA synthesized by ball milling. A sample of 30 mg of the prepared photocatalyst was added to solutions of phenol or methyl orange dye (50 mL,

Table 1
Liquid conditions of tests.

Condition	Solution	Name
Liquid-free route	Neat	TpMA _{NEAT}
Solvent-assisted route	(a) mesitylene/1,4-dioxane/3 M acetic acid: 5/5/1 (b) DMSO (c) Ultrapure water	TpMA _{S1} TpMA _{S2} TpMA _{S3}
Catalyst-assisted route	<i>p</i> -toluenesulfonic acid (PTSA) and ultrapure water	TpMA _C

10 mg/L) then the suspension was magnetically stirred in the dark for 1 h to reach steady state of adsorption-desorption prior to illumination. A 300 W Xe lamp was used as the source of light along with a 400 nm cut-off glass filter for removal of wavelengths that were not environmentally relevant. During irradiation, 1.5 mL of the solution was taken out at given intervals and immediately centrifuged. The supernatant was analyzed by use of high performance liquid chromatography (for phenol) or UV–vis light spectrophotometer (for methyl orange). To evaluate the stability of the photocatalyst, four consecutive experiments were carried out. After each run, the photocatalyst TpMA was collected using centrifugation and washed with ultrapure water, then dried at 60 °C overnight, finally reutilized in the next run under the same experimental condition. Mineralization of the contaminants was also investigated by measuring total organic carbon (TOC).

Furthermore, in order to determine the main active species in photocatalysis, radical-trapping experiments were conducted: tert-butanol (tBA), *p*-benzoquinone (BQ) and ethylenediaminetetraacetic acid disodium salt (EDTA-2Na) were used as scavengers of hydroxyl radicals ($\cdot\text{OH}$), superoxide radicals ($\cdot\text{O}_2^-$), and holes (h^+), respectively.

3. Results and discussion

3.1. Characterization

The chemical composition of the as-prepared TpMA materials using ball milling method were confirmed by elemental analysis. Ranges of C, N, O and H in TpMA synthesized by use of three ball milling routes were 50.58%~51.74%, 25.50%~32.43%, 15.82%~18.18% and 1.12%~4.72% (Table S1). These proportions were in agreement with the theoretical values calculated based on $\text{C}_{12}\text{H}_6\text{N}_6\text{O}_3$ (C-51.07%; N-29.78%; O-17.01% and H-2.14%).

TEM, SEM images and XRD patterns of these materials synthesized with mechanochemical method showed that TpMA prepared without solvent or with 1 mL solvents in the absence of *p*-toluenesulfonic acid (PTSA) had poor crystalline and morphology. With the addition of PTSA, TpMA ($\text{TpMA}_{\text{C}(1\text{mL})}$) with good crystalline and well-defined interwoven thread shape was obtained, whose mean diameter ranged in 60–100 nm (Fig. 1b, d). This result suggested the important role of PTSA

on mechanochemical preparation of TpMA. Firstly, acidic protons of PTSA protonated the primary nitrogen atoms of the amines on the MA, and then PTSA-amine salt was generated, which acted as a template. Then Tp replaced the existing PTSA unit by breaking the weaker H-bonding interaction and a stable covalent bond was formed [34]. As the volume of solvents increased to 3 mL, the obtained $\text{TpMA}_{\text{S}(3\text{mL})}$ (included $\text{TpMA}_{\text{S}1(3\text{mL})}$, $\text{TpMA}_{\text{S}2(3\text{mL})}$, $\text{TpMA}_{\text{S}3(3\text{mL})}$) and $\text{TpMA}_{\text{C}(3\text{mL})}$ exhibited similar thin ribbon-like morphologies. The characteristic diffraction peaks of TpMA could be observed in the XRD patterns of these materials (Figs. 1c, e and S2). These results indicated that TpMA prepared with identical volumes of solvents showed similar morphologies no matter what kind of solvents were used. The much more efficient formation of TpMA with 3 mL of different solvents than with 1 mL of solvents could be attributed to the dissimilarity of grinding efficiency in different amounts of reactants of liquids during ball milling. A possible reason was that, higher amount of liquid (3 mL) resulted in the solid material being more viscous, which was easier to be trapped between colliding balls during high energy ball milling process. Based on the analysis above, catalyst-assisted route is a more appropriate method to synthesize TpMA by ball milling within three hours.

To further verify the chemical composition of $\text{TpMA}_{\text{C}(3\text{mL})}$, Fourier transform infrared spectroscopy (FT-IR), and X-ray photoelectron spectroscopy (XPS) analysis were investigated. In the infrared spectrum of melamine (MA), peaks at 3462, 3413, 3343 cm^{-1} were associated with the stretching vibrations of N–H, and peaks at 1652, 1557 and 1442 cm^{-1} were assigned to stretching vibrations of Ar–C = N and C–N [35] (Fig. 2a). In the infrared spectrum of 1,3,5-triformylphloroglucinol (Tp), the adsorption peaks at 2883 and 1637 cm^{-1} were caused by stretching vibrations of C–H and C=O which were attributed to the carbonyl function of the aldehydes [36]. Stretching vibration peaks from those bands disappeared or decreased upon reaction of Tp with MA. Due to the terminal aldehyde and amines of edges of TpMA, broad bands were present at 3349 and 3209 cm^{-1} . The strong characteristic peaks corresponding to the stretching vibration of the keto-form were observed at 1615 cm^{-1} (C=O) and 1528 cm^{-1} (C=C). In addition, the peak at 1247 cm^{-1} was observed because of the newly formed C–N bond of the TpMA framework [33]. The full XPS spectrum had three peaks with binding energies of 284.6 eV, 397.9 eV and 532.8 eV,

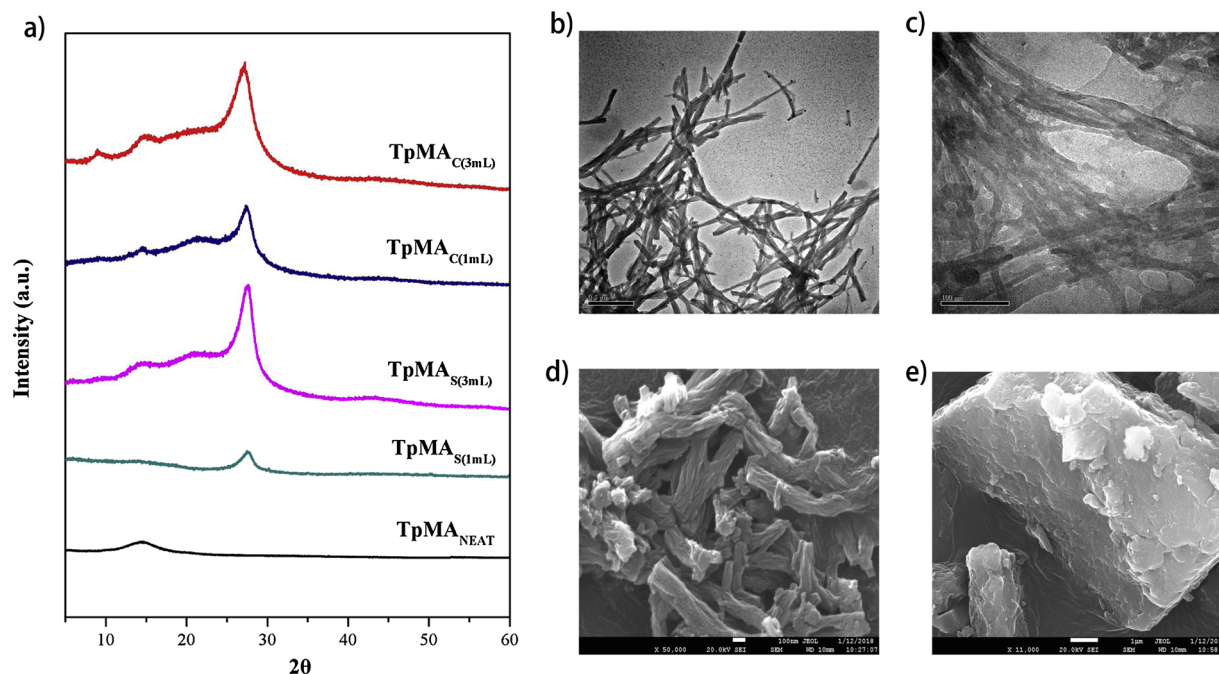


Fig. 1. PAXRD patterns for TpMA synthesized via the ball milling method with different liquids (a), TEM images of $\text{TpMA}_{\text{C}(1\text{mL})}$ (b) and $\text{TpMA}_{\text{C}(3\text{mL})}$ (c), SEM of $\text{TpMA}_{\text{C}(1\text{mL})}$ (d) and $\text{TpMA}_{\text{C}(3\text{mL})}$ (e).

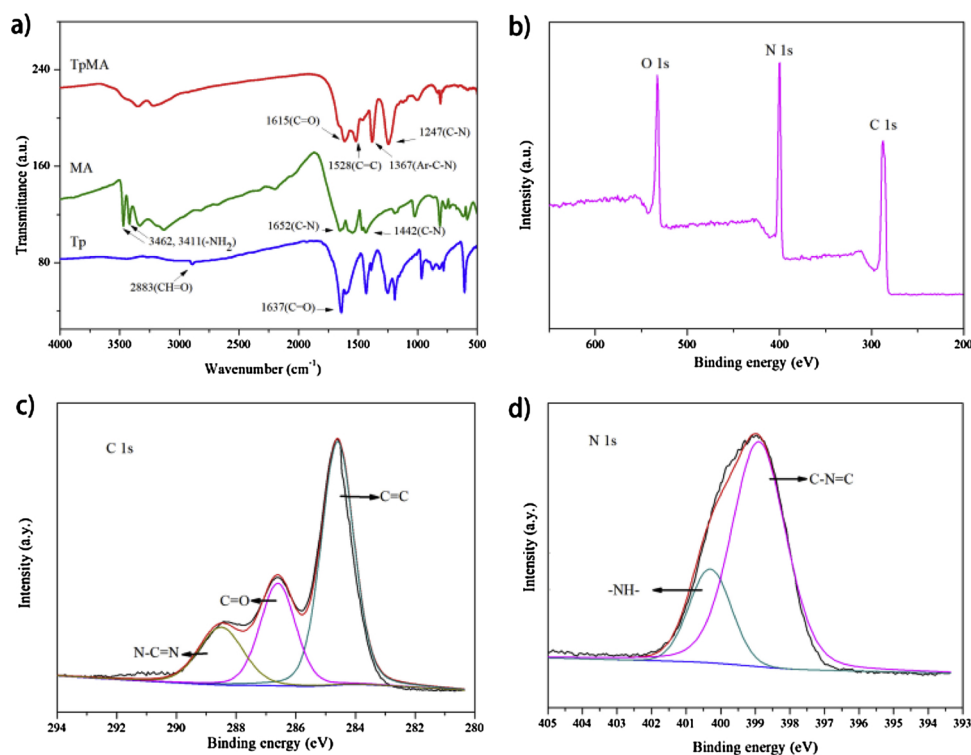


Fig. 2. Fourier transform infrared spectroscopy spectra of Tp, MA and TpMA_{C(3mL)} (a), XPS survey spectrum (b), high-resolution spectra of C 1s (c), and high-resolution spectra of N 1s of TpMA_{C(3mL)} (d).

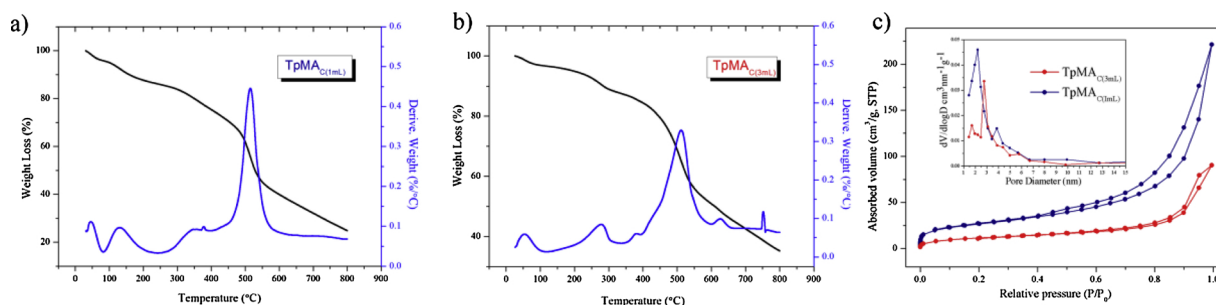


Fig. 3. Thermogravimetric analysis (TGA) profile of as-prepared TpMA_{C(1mL)} (a) and TpMA_{C(3mL)} (b), Nitrogen adsorption-desorption isotherms of TpMA_{C(1mL)} and TpMA_{C(3mL)}, and the inset is the distribution of pore diameter (c).

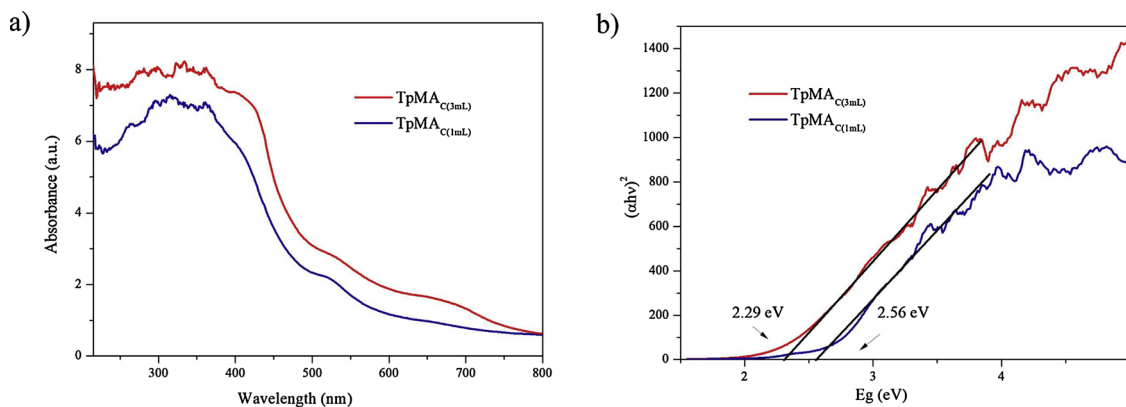


Fig. 4. UV-vis diffuse reflectance spectra (a), and band gap energy (b) of TpMA_{C(1mL)} and TpMA_{C(3mL)}.

corresponding to C 1s, N 1s and O 1s, respectively [18] (Fig. 2b). XPS provides an analysis for elements in the outer 10 nm of a surface, and elemental analysis can quantify elements both in surface and inner of the materials. Elemental compositions of TpMA based on the C/N

atomic ratio calculated from XPS (1.683) were analogous to that determined by elemental analysis (1.766). This result indicated that functional groups of samples synthesized by ball milling method were homogeneous. The C 1s in high-resolution XPS spectrum of TpMA,

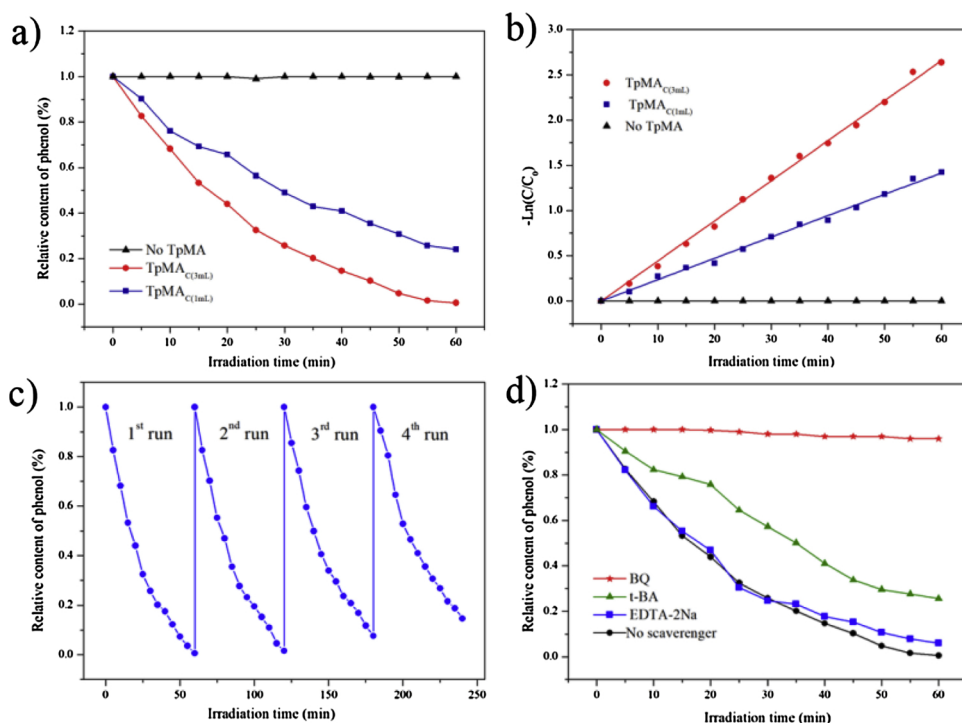


Fig. 5. Photo-catalytic degradation of phenol under visible light irradiation (a), linear simulation $-\ln(C/C_0) = kt$ of the kinetic curves for phenol degradation (b), recycling runs of $\text{TpMA}_{\text{C}(3\text{mL})}$ (c), effects of scavengers on the photocatalytic degradation of phenol catalyzed by $\text{TpMA}_{\text{C}(3\text{mL})}$ (d). The initial concentration of phenol was 10 mg/L.

which could be fitted into three peaks with binding energies of 284.5 eV, 286.6 eV and 288.5 eV, represented carbon atoms in the linkage ($\text{sp}^2 \text{C}=\text{C}$ and $\text{C}=\text{O}$) and in the triazine ring ($\text{N}-\text{C}=\text{N}$) [37], respectively (Fig. 2c). The characteristic peak of N 1s was assigned to two groups as triazine groups ($\text{C}-\text{N}=\text{C}$) at 398.9 eV and $-\text{NH}-$ groups at 400.3 eV. FT-IR and XPS spectra of the as-synthesized TpMA matched well to those of solvo-thermally synthesized counterparts reported previously [32].

Thermogravimetric analysis (TGA) of $\text{TpMA}_{\text{C}(1\text{mL})}$ and $\text{TpMA}_{\text{C}(3\text{mL})}$ prepared by ball milling were investigated in the temperature range between 10 and 800 °C with heating rate of 10 °C min^{-1} in N_2 atmosphere (Fig. 3a, b). The $\text{TpMA}_{\text{C}(1\text{mL})}$ and $\text{TpMA}_{\text{C}(3\text{mL})}$ samples showed thermal stabilities until the temperature was up to 518 °C. In the range of 10–100 °C, the small weight loss was due to volatilization of surface adsorbed water molecules. They started to gradually degrade above 100 °C. In the range of approximately 100–300 °C, the weight-loss was 16.5% weight and 10.9% for $\text{TpMA}_{\text{C}(1\text{mL})}$ and $\text{TpMA}_{\text{C}(3\text{mL})}$, respectively. The two materials continued to decompose between 300–518 °C with losses of mass of 54.8% ($\text{TpMA}_{\text{C}(1\text{mL})}$) and 36.8% ($\text{TpMA}_{\text{C}(3\text{mL})}$). Finally, losses of mass of 72.2% and 65.2% were observed for $\text{TpMA}_{\text{C}(1\text{mL})}$ and $\text{TpMA}_{\text{C}(3\text{mL})}$, respectively as the temperature was up to 800 °C because of the decomposition of the framework. It was obvious that, $\text{TpMA}_{\text{C}(1\text{mL})}$ exhibited more serious weight loss than $\text{TpMA}_{\text{C}(3\text{mL})}$, which proved the higher thermal stability of $\text{TpMA}_{\text{C}(3\text{mL})}$ than $\text{TpMA}_{\text{C}(1\text{mL})}$. Architectural rigidity and permanent porosity of $\text{TpMA}_{\text{C}(1\text{mL})}$ and $\text{TpMA}_{\text{C}(3\text{mL})}$ were determined by N_2 adsorption-desorption analysis at 77 K. It can be seen from Fig. 3c that the N_2 adsorption/desorption isotherms of the two materials belonged to type IV isotherm according to the IUPAC (International Union of Pure and Applied Chemistry) classification, which was characteristic of mesoporous solids. The Brunauer-Emmett-Teller (BET) surface areas and pore volume of $\text{TpMA}_{\text{C}(1\text{mL})}$ and $\text{TpMA}_{\text{C}(3\text{mL})}$ were 102.4 m^2/g , 0.342 cc/g and 82.3 m^2/g , 0.091 cc/g , respectively. The pore size distribution plot in Fig. 3c inset showed that $\text{TpMA}_{\text{C}(1\text{mL})}$ and $\text{TpMA}_{\text{C}(3\text{mL})}$ both possessed mesopores (2.2 to 2.7 nm).

Optical properties of the synthesized-products were investigated via the absorption and reflectance spectra of the powders in the wavelength range 200–800 nm using UV–vis diffuse reflection spectroscopy (DRS) (Fig. 4a). Both $\text{TpMA}_{\text{C}(1\text{mL})}$ and $\text{TpMA}_{\text{C}(3\text{mL})}$ responded to visible light,

and their optical absorption edges were located at about 521 and 542 nm and the steep shape were caused by band gap transitions. The optical absorption edge of $\text{TpMA}_{\text{C}(3\text{mL})}$, compared to $\text{TpMA}_{\text{C}(1\text{mL})}$ exhibited red shift, illustrating that $\text{TpMA}_{\text{C}(3\text{mL})}$ produced by more efficient grinding could have been excited during irradiation with visible light and then generated more charge carries. Optical band gap energies (E_g) were calculated according to Eq. 1 [34,38,39].

$$(\alpha h\nu)^{n/2} = A(h\nu - E_g) \quad (1)$$

where α represents the absorption coefficient, $h\nu$ is the photon energy, n is the power index determined by the type of optical transition, $n = 1$ for direct transition and $n = 4$ for indirect transition, A is a constant, E_g is the band gap energy. Here the absorption coefficient (α) was replaced by absorbance (Abs) because the concentration and the optical path length are invariable [39]. By plotting $(\alpha h\nu)^2$ versus $h\nu$, and extrapolating the straight line to the $h\nu$ axis, band gap values for $\text{TpMA}_{\text{C}(1\text{mL})}$ and $\text{TpMA}_{\text{C}(3\text{mL})}$ were estimated to be 2.56 and 2.29 eV, respectively (Fig. 4b). Based on that result, it can be concluded that the simple ball milling method resulted in materials with a suitable band gap energy as materials produced by use of the traditional solvothermal method did (the band gap energy was estimated to be 2.30 eV) [33].

3.2. Photocatalytic activity

The photo-catalytic activity of TpMA was investigated by degrading 10 mg/L phenol as a model environmental pollutant under irradiation with visible light. The removal efficiency of phenol was not exceeding 12% without light irradiation, indicating that TpMA had low adsorption ability to phenol. $\text{TpMA}_{\text{C}(3\text{mL})}$ could completely catalytic degrade phenol after 60 min irradiation, whereas about 83.5% phenol was decomposed catalyzed by $\text{TpMA}_{\text{C}(1\text{mL})}$. $\text{TpMA}_{\text{C}(3\text{mL})}$ exhibited better photocatalytic performance than $\text{TpMA}_{\text{C}(1\text{mL})}$ toward the degradation of phenol (Fig. 5a). Total organic carbon (TOC) further confirmed that 43.2% ($\text{TpMA}_{\text{C}(1\text{mL})}$) and 45.6% ($\text{TpMA}_{\text{C}(3\text{mL})}$) of phenol was mineralized after photocatalytic reaction. Catalytic photo-degradation of methyl orange was consistent with that of phenol, 89% and 79% of methyl orange was photo-degraded after 60 min irradiation with visible light in the presence of $\text{TpMA}_{\text{C}(3\text{mL})}$ and $\text{TpMA}_{\text{C}(1\text{mL})}$, respectively.

Table 2
The comparison of solvothermal and mechanochemical synthetic process.

Materials	Synthetic method	Total quality of raw materials (mg)	Liquid additive during grinding (mL)	solid-to-liquid ratio ^a (mg/mL)	Temperature	Preparation time	performance and characteristics of the materials	ref
TpPa-1	ST ¹	1, 3, 5-Triformylphloroglucinol (Tp) (63 mg), Paraphenylenediamine (Pa-1) (48 mg)	1.5 mL of mesitylene, 1.5 mL of dioxane, 0.5 mL of 3 M aqueous acetic acid Solvent-free	31.71	120 °C	72 hours	flowerlike morphology; surface area: 535 m ² /g.	[40,36]
	MC ²			–	room temperature	45 min	moderate crystallinity; spherical-shaped particles; surface area: 61 m ² /g; remarkably stable in boiling water, acid (9 N HCl), and base (3 N NaOH).	
TpPa-2	ST	1, 3, 5-triformylphloroglucinol (Tp) (63 mg), 2,5-dimethylparaph enylenediamine (Pa-2) (61 mg)	1.5 mL of mesitylene, 1.5 mL of dioxane, 0.5 mL of 3 M aqueous acetic acid Solvent-free	35.43	120 °C	72 hours	flowerlike morphology; surface area: 339 m ² /g.	
	MC			–	room temperature	45 min	moderate crystallinity; spherical-shaped particles; surface area: 56 m ² /g; remarkably stable in boiling water, acid (9 N HCl), and base (3 N NaOH).	
TpBD	ST	1, 3, 5-Triformylphloroglucinol (Tp) (63 mg), Benzidine (BD) (82.9 mg)	1.5 mL of mesitylene, 1.5 mL of dioxane, 0.5 mL of 3 M aqueous acetic acid Solvent-free	41.69	120 °C	72 hours	flowerlike morphology; surface area: 537 m ² /g.	
	MC			–	room temperature	45 min	moderate crystallinity; graphene-sheet-like layered Morphology; surface area: 35 m ² /g; remarkably stable in boiling water, acid (9 N HCl), and base (3 N NaOH).	[24]
TpTh	ST	1, 3, 5-Triformylphloroglucinol (Tp) (63.0 mg), phenyl hydrazide (Ph) (97.2 mg)	3.0 mL of mesitylene, 1.5 mL of dioxane, 0.5 mL of 3 M aqueous acetic acid 1–2 drop (~100 µL) of mesitylene : dioxane (2:1) and 1 drop (~50 µL) of 3 M acetic acid/	32.04	120 °C	72 hours	layer like morphology.	
	MC			1068	room temperature	90 min	layer like morphology; Low surface area; identical thermal stability.	
DhaTph	ST	2,5-dihydroxyterephthalaldehyde (Dha) (13.3 mg), tetra(p-amino-phenyl)porphyrin (Tph) (27.0 mg)	6 M acetic acid (0.2 mL), dichlorobenzene and ethanol (1:1) (2 mL).	18.32	120 °C	72 hours	square shaped particles; surface area: 1305 m ² /g; high water and acid (3n HCl for 7 days) stability.	[30,24]
	MC		6 M acetic acid (1 drop), dichlorobenzene, ethanol (1:1) (2 drop)	268.67	room temperature	90 min	square shaped particles; Low surface area; Decomposed in acid (3 N HCl for 3days).	
LZU-1	ST	1,3,5-triformylbenzene (TFB) (48 mg), 1,4-diaminobenzene (Pa-1) (48 mg)	1,4-dioxane (3.0 mL), 0.6 mL of 3 M aqueous acetic acid	26.67	120 °C	72 hours	layered-sheet morphology; surface area: 410 m ² /g; Not stable in water.	[41,24]
	MC		1–2 drop of mesitylene : dioxane (1:1) and 1 drop of 3 M acetic acid	640	room temperature	90 min	thin ribbon shaped structures; Not stable in water; Low surface area.	
TpBpy	ST	1,3,5-triformylphloroglucinol(Tp) (63 mg), 2,2'-bipyridine-5,5'-diamine(Bpy) (83.7 mg)	0.6 mL of 6 M aqueous acetic acid	22.23	120 °C	72 hours	thread-like morphology; surface area: 1746 m ² /g.	[42]
	MC		60 µL of DMAc, 30 µmLof o-DCB, 15 µLof 6 M acetic acid	1397.14	room temperature	90 min	sheet-like morphology; surface area: 293 m ² /g; lower crystallinity and porosity; similar proton conducting behaviour; More compact pellet that could effectively separate the gases apart.	
TpMA	ST	1,3,5-Triformylphloroglucinol (Tp) (105 mg), melamine (MA) (63 mg)	mesitylene/1,4-dioxane/3 M acetic acid (5/5/1 by vol.; 11.0 mL)	15.27	120 °C	72 hours	thread-like morphology; surface area: 56.9 m ² /g; 90% of phenol was photodegraded with TpMA after 40 min - irradiation; retained photocatalytic ability of 86.8% after recycling four times.	[33]
	MC		p-toluenesulfonic acid (PTSA) (3 mL)	119.67	room temperature	3 hours	exfoliative ribbon-like structures; surface area: 82.3 m ² /g; completely catalytic degrade phenol after 60 min irradiation retained photocatalytic ability of 87.6% after recycling four times.	This work

* Solid-to-liquid ratio means the ratio of raw materials quality to liquid additive. The larger the ratio, the less solvent is needed in the reaction.

¹ ST is the abbreviation of solvothermal synthesis.

² MC is the abbreviation of mechanochemical synthesis.

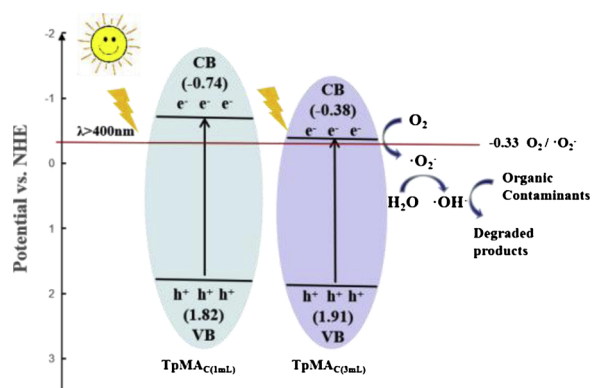


Fig. 6. Mechanism of $\text{TpMA}_{\text{C}(1\text{mL})}$ and $\text{TpMA}_{\text{C}(3\text{mL})}$ in photocatalytic degradation of organic contaminants.

To further understand reaction kinetics for phenol and methyl orange under irradiation with visible light, experimental data was fitted by a pseudo-first-order kinetic equation (Eq. 2) [33].

$$-\ln(C/C_0) = kt, \quad (2)$$

where C and C_0 are the concentrations of phenol (or methyl orange) corresponding to the irradiation time t and 0, respectively. k is the photodegradation rate constant. $\text{TpMA}_{\text{C}(3\text{mL})}$ resulted in a high rate constant of 0.044 L/mg/min , which was approximately 2-fold greater than that of $\text{TpMA}_{\text{C}(1\text{mL})}$ (0.023 L/mg-min) (Fig. 5b). Reaction rates of phenol and methyl orange photodegradation catalyzed by $\text{TpMA}_{\text{C}(3\text{mL})}$ were comparable with those catalyzed by the photocatalyst prepared with the solvo-thermal method [32]. The reaction time and organic solvents consumed to prepare TpMA was shortened significantly. In comparison with solvothermal synthesis, ball milling is potentially a scalable low-cost method of producing COFs (Table 2). To evaluate the stability and recyclability of the TpMA photocatalyst, consecutive experiments of phenol photodegradation were conducted (Fig. 6).

$\text{TpMA}_{\text{C}(3\text{mL})}$ retained 87.6% photocatalytic ability after recycling four times, which illustrated that TpMA which was prepared by mechanochemical method exhibit sufficient recyclability and stability (Fig. 5c).

3.3. Mechanism of photocatalytic activity

When the trapping experiments were performed to elucidate the photocatalytic mechanism of TpMA through analysis of the roles of reactive species in photocatalysis process, P-benzoquinone (BQ), tert-butanol (tBA), and ethylenediaminetetraacetic acid disodium salt (EDTA-2Na) were applied as scavengers to quench $\cdot\text{O}_2^-$, $\cdot\text{OH}$ radicals and holes (h^+), respectively [43]. Compared to the absence of scavengers, degradation of phenol photo-catalyzed by $\text{TpMA}_{\text{C}(3\text{mL})}$ was decreased to nearly zero in the presence of BQ (Fig. 5d). Besides, the degradation efficiency of phenol decreased to 74.5% with the addition of tBA, while no change was observed when EDTA-2Na was added. These results indicated that $\cdot\text{O}_2^-$ and $\cdot\text{OH}$ radicals might be involved in photocatalytic decomposition of phenol and that $\cdot\text{O}_2^-$ served as the primary radical. Band gaps of $\text{TpMA}_{\text{C}(1\text{mL})}$ and $\text{TpMA}_{\text{C}(3\text{mL})}$ were 2.56 and 2.29 eV respectively, and band positions were calculated by valence band X-ray photo-electron spectroscopy (VB XPS) [44–46]. VB edges of $\text{TpMA}_{\text{C}(1\text{mL})}$ and $\text{TpMA}_{\text{C}(3\text{mL})}$ were determined to be 1.82 eV and 1.91 eV, and CB potentials (E_{CB}) were -0.74 and -0.38 eV, respectively. (Eq. 3) (Fig. 7a).

$$E_{\text{CB}} = E_{\text{VB}} - E_{\text{g}} \quad (3)$$

Therefore, a possible photo-degradation mechanism for phenol was considered that when photons energy from illumination was greater than or equal to the band gap of TpMA ($\geq 2.56 \text{ eV}$ for $\text{TpMA}_{\text{C}(1\text{mL})}$ or $\geq 2.29 \text{ eV}$ for $\text{TpMA}_{\text{C}(3\text{mL})}$), electron-hole pairs were excited and generated. Excess photoinduced electrons were separated and migrated from VB to the CB and enriched CB electrons could readily transfer to the surface of TpMA and react with dissolved oxygen molecules to form abundant $\cdot\text{O}_2^-$ radicals, then $\cdot\text{O}_2^-$ oxidize H_2O molecules to further produce active $\cdot\text{OH}$ that could then participate in indirect, photo-

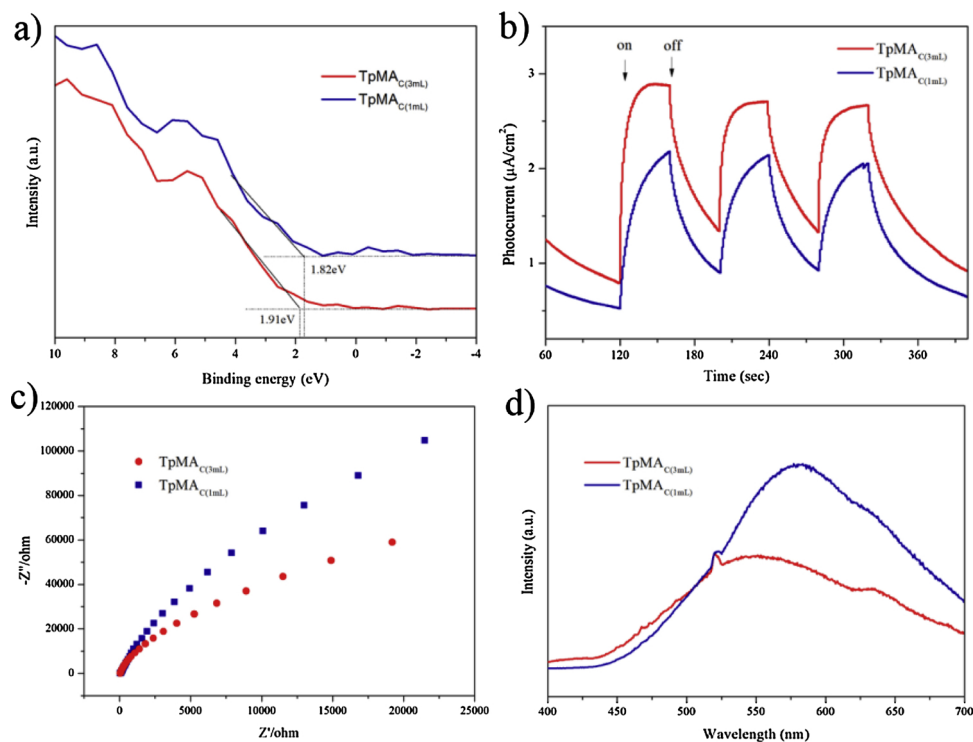


Fig. 7. Valence band X-ray photoelectron spectroscopy (a), transient photocurrent responses of plots (b), EIS Nyquist (c), and photoluminescence (PL) spectra (d) of $\text{TpMA}_{\text{C}(1\text{mL})}$ and $\text{TpMA}_{\text{C}(3\text{mL})}$.

catalytic degradation reaction of organics (Fig. 6). Besides, comparison of the band positions showed that TpMA_{C(3mL)} was more positive than that of TpMA_{C(1mL)}, which endowed TpMA_{C(3mL)} with enhanced photodegradation capability for pollutants.

In order to estimate rates of transfer of photo-generated charge pairs, photocurrent responses were measured via a standard three-electrode system [47]. When photo-generated electron-hole pairs were separated, photocurrent was detected. Under irradiation with visible light, the photocurrent response of TpMA_{C(3mL)} was greater than that of TpMA_{C(1mL)} (Fig. 7b). This result suggested that the photoexcited electron-hole pairs of TpMA_{C(3mL)} have greater separation efficiency and lesser rates of recombination. Electro-chemical impedance spectroscopy (EIS) of the photo-catalysts was performed to further prove the photo-generated carriers migration [48]. The EIS was measured under the same conditions as used during the photocurrent experiment, and its frequency ranged from 100 kHz to 0.1 Hz with an amplitude of the sinusoidal wave of 50 mV. Arc radii Nyquist plots were related to reaction rates of at the surface of the electrode (Fig. 7c). The radius of TpMA_{C(3mL)} occurred to be smaller than that of TpMA_{C(1mL)}, which indicated that lesser solid-state interface layer resistance and charge transfer resistance on the surface. Hence, the interfacial charge of TpMA_{C(3mL)} could transfer more rapidly, which leads to effective separation of photogenerated electron-hole pairs.

Photocatalytic activity of TpMA was related to not only transfer of electrons, but also rates of recombination of photo-generated charge carriers. Efficiency of separation of electron-hole pairs was provided by photoluminescence (PL) spectra, and the high intensity revealed an increased recombination rate of photogenerated charge carriers. Broad luminescence bands around 560–580 nm were observed in PL measurements of TpMA_{C(1mL)} and TpMA_{C(3mL)} (Fig. 7d), and the peak intensity of TpMA_{C(3mL)} in the PL spectrum was less than that of the TpMA_{C(1mL)}. This result indicated that electron-hole recombination of TpMA_{C(3mL)} was inhibited and separation efficiency of the photo-generated charge pairs increased. The result is consistent with measurements of photocurrent and EIS. Greater rates of electron transfer and lesser rates of recombination of electron-hole pairs urge more radicals to react with the pollutants on the surface of photocatalysts and boost the photocatalytic activity.

TpMA_{C(3mL)} was synthesized with assistance of appropriate catalysts during mechanochemical grinding, which promoted the reactant diffusion rate in a liquid interparticle zone, and ultimately formed a thin ribbon-like structure. Through analysis of generation, separation, and migration of photoexcited electron-hole pairs in photocatalytic reaction above, it was concluded that under irradiation with visible light, compared to TpMA_{C(1mL)}, the ribbon-like TpMA_{C(3mL)} could effectively enhance separation and migration performance of photogenerated electron-hole pairs, which results in an enhanced photocatalytic efficiency.

4. Conclusions

In summary, for the first time, chemically stable covalent organic frameworks of TpMA based on modified Schiff base reaction between 1,3,5-triformylphloroglucinol (Tp) and melamine (MA) via a simple, room-temperature mechanochemical synthetic method were produced. Addition of liquids, especially catalysts during formation can improve crystallinity of the COF materials. Under three hours reaction, different solvents or amount of catalyst added (1 or 3 mL) during ball milling resulted in two morphologies, they were interwoven thread-shaped and exfoliative thin ribbon-like structures. Comparing their photo-chemical properties, the ribbon-like TpMA_{C(3mL)} has more efficient charge transport and separate properties, that leads to exhibited remarkable photocatalytic activity towards water purification under visible light, and retained 87.6% of initial photodegradation after being used four times. Rates of reaction of TpMA_{C(3mL)} for degrading phenol were comparable with those of TpMA prepared by the solvothermal method.

Although the crystallinity of the mechano-chemically synthesized TpMA COFs were moderate in comparison to that of using solvothermal synthesis, the approach indeed has many advantages: a) it substantially contributed to the material yield and reaction rate at ambient temperature; b) the scalable features of the approach provide an alternative way for the synthesis of the COFs; c) usage of a minimal amount of solvents makes it green and environmentally friendly. The rapid mechanochemical approach provides an alternative way for the synthesis of COFs. It is a promising potential tool for industrial scale production of COFs, which will make greater use of COFs for environmental pollution abatement. We hope our strategy will provide a convenient reference for large scale production of stable and functional COF materials.

Acknowledgements

This work was jointly supported by National Key Research and Development Program of China (2016YFA0203100), the National Natural Science Foundation of China (21537004, 41673131, 21777169, 21621064), and Strategic Priority Research Program of the Chinese Academy of Sciences (XDB14010201).

Appendix A. Supplementary data

Supplementary material related to this article can be found, in the online version, at doi:<https://doi.org/10.1016/j.jhazmat.2019.02.046>.

References

- [1] Z. Luo, S. Fan, J. Liu, W. Liu, X. Shen, C. Wu, Y. Huang, G. Huang, H. Huang, M. Zheng, A 3D stable metal-organic framework for highly efficient adsorption and removal of drug contaminants from water, *Polymers* 10 (2) (2018) 209.
- [2] J. Liu, G. Liu, C. Gu, W. Liu, J. Xu, B. Li, W. Wang, Rational synthesis of a novel 3,3,5-c polyhedral metal-organic framework with high thermal stability and hydrogen storage capability, *J. Mater. Chem.* 4 (30) (2016) 11630–11634.
- [3] W. Liu, X. Shen, Y. Han, Z. Liu, W. Dai, A. Dutta, A. Kumar, J. Liu, Selective adsorption and removal of drug contaminants by using an extremely stable Cu(II)-based 3D metal-organic framework, *Chemosphere* 215 (2019) 524–531.
- [4] D. Huang, Z. Li, G. Zeng, C. Zhou, W. Xue, X. Gong, X. Yan, S. Chen, W. Wang, M. Cheng, Megamerger in photocatalytic field: 2D g-C₃N₄ nanosheets serve as support of OD nanomaterials for improving photocatalytic performance, *Appl. Catal. B Environ.* 240 (2019) 153–173.
- [5] D. Huang, X. Yan, M. Yan, G. Zeng, C. Zhou, J. Wan, M. Cheng, W. Xue, Graphitic carbon nitride-based heterojunction photoactive nanocomposites: applications and mechanism insight, *ACS Appl. Mater. Interfaces* 10 (25) (2018) 21035–21055.
- [6] C.S. Diercks, O.M. Yaghi, The atom, the molecule, and the covalent organic framework, *Science* 355 (6328) (2017) ea11585.
- [7] S. Das, P. Heasman, T. Ben, S. Qiu, Porous organic materials: strategic design and structure-function correlation, *Chem. Rev.* 117 (3) (2017) 1515–1563.
- [8] A.P. Côté, A.I. Benin, N.W. Ockwig, A.J. Matzger, M. O’Keeffe, O.M. Yaghi, Porous, crystalline, covalent organic frameworks, *Science* 310 (5751) (2005) 1166–1170.
- [9] S. Ding, W. Wang, Covalent organic frameworks (COFs): from design to applications, *Chem. Soc. Rev.* 42 (2) (2013) 548–568.
- [10] H.M. El-Kaderi, J.R. Hunt, J.L. Mendoza-Cortés, A.P. Côté, R.E. Taylor, M. O’Keeffe, O.M. Yaghi, Designed synthesis of 3D covalent organic frameworks, *Science* 316 (2007) 268–272.
- [11] A.P. Côté, H.M. El-Kaderi, H. Furukawa, J.R. Hunt, O.M. Yaghi, Reticular synthesis of microporous and mesoporous 2D covalent organic frameworks, *J. Am. Chem. Soc.* 129 (2007) 12914–12915.
- [12] S.S. Han, H. Furukawa, O.M. Yaghi, W.A. Goddard III, Covalent organic frameworks as exceptional hydrogen storage materials, *J. Am. Chem. Soc.* 130 (35) (2008) 11580–11581.
- [13] C.D. Wood, B. Tan, A. Trewin, H.J. Niu, D. Bradshaw, M.J. Rosseinsky, Y.Z. Khimyak, N.L. Campbell, R. Kirk, E. Stöckel, A.I. Cooper, Hydrogen storage in microporous hypercrosslinked organic polymer networks, *Chem. Mater.* 19 (8) (2007) 2034–2048.
- [14] N.B. McKeown, P.M. Budd, Polymers of intrinsic microporosity (PIMs): organic materials for membrane separations, heterogeneous catalysis and hydrogen storage, *Chem. Soc. Rev.* 35 (2006) 675–683.
- [15] G. Kupgan, L.J. Abbott, K.E. Hart, C.M. Colina, Modeling amorphous microporous polymers for CO₂ capture and separations, *Chem. Rev.* 118 (11) (2018) 5488–5538.
- [16] X. Wang, X. Han, J. Zhang, X. Wu, Y. Liu, Y. Cui, Homochiral 2D porous covalent organic frameworks for heterogeneous asymmetric catalysis, *J. Am. Chem. Soc.* 138 (38) (2016) 12332–12335.
- [17] M. Bhadra, H.S. Sasmal, A. Basu, S.P. Midya, S. Kandambeth, P. Pachfule, E. Balaraman, R. Banerjee, Predesigned metal-anchored building block for in situ generation of Pd nanoparticles in porous covalent organic framework: application

- in heterogeneous tandem catalysis, *ACS Appl. Mater. Interfaces* 9 (15) (2017) 13785–13792.
- [18] B. He, W. Li, A. Lu, High nitrogen-content carbon nanosheets formed using the Schiff-base reaction in a molten salt medium as efficient anode materials for lithium-ion batteries, *J. Mater. Chem. A* 3 (2015) 579–585.
- [19] B. Sun, J. Li, W. Dong, M. Wu, D. Wang, Selective growth of covalent organic framework ultrathin films on hexagonal boron nitride, *J. Phys. Chem. C* 120 (2016) 14706–14711.
- [20] B. Yao, J. Li, N. Huang, J. Kan, L. Qiao, L. Ding, F. Li, Y. Dong, Pd NP-Loaded and covalently cross-linked COF membrane microreactor for aqueous CBs dechlorination at room temperature, *ACS Appl. Mater. Interfaces* 10 (24) (2018) 20448–20457.
- [21] S. Ding, W. Wang, Covalent organic frameworks (COFs): from design to applications, *Chem. Soc. Rev.* 42 (2) (2013) 548–568.
- [22] P. Zhang, S. Dai, Mechanochemical synthesis of porous organic materials, *J. Mater. Chem. A* 5 (31) (2017) 16118–16127.
- [23] Z. Xiang, D. Cao, L. Dai, Well-defined two dimensional covalent organic polymers: rational design, controlled syntheses, and potential applications, *Polym. Chem.* 6 (2015) 1896–1991.
- [24] G. Das, D.B. Shinde, S. Kandambeth, B.P. Biswal, R. Banerjee, Mechanochemical synthesis of imine, beta-ketoenamine, and hydrogen-bonded imine-linked covalent organic frameworks using liquid-assisted grinding, *Chem. Commun.* 50 (84) (2014) 12615–12618.
- [25] A.M. Elseman, M.M. Rashad, A.M. Hassan, Easily attainable, efficient solar cell with mass yield of nanorod single-crystalline organo-metal halide perovskite based on a ball milling technique, *ACS Sustain. Chem. Eng.* 4 (9) (2016) 4875–4886.
- [26] H. Lyu, B. Gao, F. He, C. Ding, J. Tang, J.C. Crittenden, Ball-milled carbon nanomaterials for energy and environmental applications, *ACS Sustain. Chem. Eng.* 5 (11) (2017) 9568–9585.
- [27] R.E. Morris, S.L. James, Solventless synthesis of zeolites, *Angew. Chem., Int. Ed.* 52 (2013) 2163–2165.
- [28] P.A. Julien, K. Užarević, A.D. Katsenis, S.A.J. Kimber, T. Wang, O.K. Farha, Y. Zhang, J. Casaban, L.S. Germann, M. Etter, R.E. Dinnebier, S.L. James, I. Halasz, T. Friščić, In situ monitoring and mechanism of the mechanochemical formation of a microporous MOF-74 framework, *J. Am. Chem. Soc.* 138 (9) (2016) 2929–2932.
- [29] T. Friščić, D.G. Reid, I. Halasz, R.S. Stein, R.E. Dinnebier, M.J. Duer, Ion- and liquid-assisted grinding: improved mechanochemical synthesis of metal-organic frameworks reveals salt inclusion and anion templating, *Angew. Chem. Int. Ed.* 49 (4) (2010) 712–715.
- [30] S. Kandambeth, D.B. Shinde, M.K. Panda, B. Lukose, T. Heine, R. Banerjee, Enhancement of chemical stability and crystallinity in porphyrin-containing covalent organic frameworks by intramolecular hydrogen bonds, *Angew. Chem., Int. Ed.* 52 (49) (2013) 13052–13056.
- [31] D. Hulicova, J. Yamashita, Y. Soneida, H. Hatori, M. Kodama, Supercapacitors prepared from melamine-based carbon, *Chem. Mater.* 17 (5) (2005) 1241–1247.
- [32] M.G. Schwab, B. Fassbender, H.W. Spiess, A. Thomas, X. Feng, K. Mullen, Catalyst-free preparation of melamine-based microporous polymer networks through schiff base chemistry, *J. Am. Chem. Soc.* 131 (2009) 7216–7217.
- [33] S. He, Q. Rong, H. Niu, Y. Cai, Construction of a superior visible-light-driven photocatalyst based on a C3N4 active centre-photoelectron shift platform-electron withdrawing unit triadic structure covalent organic framework, *Chem. Commun.* 53 (69) (2017) 9636–9639.
- [34] S. Karak, S. Kandambeth, B.P. Biswal, H.S. Sasmal, S. Kumar, P. Pachfule, R. Banerjee, Constructing ultraporos covalent organic frameworks in seconds via an organic terracotta process, *J. Am. Chem. Soc.* 139 (5) (2017) 1856–1862.
- [35] N. Sahiner, S. Demirci, K. Sel, Covalent organic framework based on melamine and dibromoalkanes for versatile use, *J. Porous Mater.* 23 (4) (2016) 1025–1035.
- [36] B.P. Biswal, S. Chandra, S. Kandambeth, B. Lukose, T. Heine, R. Banerjee, Mechanochemical synthesis of chemically stable isoreticular covalent organic frameworks, *J. Am. Chem. Soc.* 135 (14) (2013) 5328–5331.
- [37] C. Tian, J. Zhao, X. Ou, J. Wan, Y. Cai, Z. Lin, Z. Dang, B. Xing, Enhanced adsorption of p-Arsanilic acid from water by amine-modified UiO-67 as examined using extended X-ray absorption fine structure, X-ray photoelectron spectroscopy, and density functional theory calculations, *Environ. Sci. Technol.* 52 (6) (2018) 3466–3475.
- [38] D. Kandi, S. Martha, A. Thirumurugan, K.M. Parida, CdS QDs-decorated self-doped γ -Bi₂MoO₆: a sustainable and versatile photocatalyst toward photoreduction of Cr (VI) and degradation of phenol, *ACS Omega* 2 (12) (2017) 9040–9056.
- [39] Y. Ao, K. Wang, P. Wang, C. Wang, J. Hou, Synthesis of novel 2D-2D p-n heterojunction BiOBr/La₂Ti₂O₇ composite photocatalyst with enhanced photocatalytic performance under both UV and visible light irradiation, *Appl. Catal. B Environ.* 194 (2016) 157–168.
- [40] S. Kandambeth, A. Mallick, B. Lukose, M.V. Mane, T. Heine, R. Banerjee, Construction of crystalline 2D covalent organic frameworks with remarkable chemical (acid/base) stability via a combined reversible and irreversible route, *J. Am. Chem. Soc.* 134 (48) (2012) 19524–19527.
- [41] S.Y. Ding, J. Gao, Q. Wang, Y. Zhang, W.G. Song, C.Y. Su, W. Wang, Construction of covalent organic framework for catalysis: Pd/COF-LZU1 in Suzuki-Miyaura coupling reaction, *J. Am. Chem. Soc.* 133 (49) (2011) 19816–19822.
- [42] D.B. Shinde, H.B. Aiyappa, M. Bhadra, B.P. Biswal, P. Wadge, S. Kandambeth, B. Garai, T. Kundu, S. Kurungot, R. Banerjee, A mechanochemically synthesized covalent organic framework as a proton-conducting solid electrolyte, *J. Mater. Chem. A Mater. Energy Sustain.* 4 (7) (2016) 2682–2690.
- [43] J. Meng, J. Pei, Z. He, et al., Facile synthesis of g-C₃N₄ nanosheets loaded with WO₃ nanoparticles with enhanced photocatalytic performance under visible light irradiation, *RSC Adv.* 7 (39) (2017) 24097–24104.
- [44] Z. Mo, X. Bai, L. Di, et al., Enhanced catalytic activity of potassium-doped graphitic carbon nitride induced by lower valence position, *Appl. Catal. B Environ.* 164 (2015) 77–81.
- [45] N. Kamarulzaman, M.F. Kasim, N.F. Chayed, Elucidation of the highest valence band and lowest conduction band shifts using XPS for ZnO and Zn_{0.99}Cu_{0.01}O band gap changes, *Results Phys.* 6 (C) (2016) 217–230.
- [46] P.D.C. King, T.D. Veal, P.H. Jefferson, et al., Unification of the electrical behavior of defects, impurities, and surface states in semiconductors: virtual gap states in CdO, *Phys. Rev. B* 79 (3) (2009) 035203.
- [47] J. Cao, Z. Yang, W. Xiong, Y. Zhou, Y. Peng, X. Li, C. Zhou, R. Xu, Y. Zhang, One-step synthesis of Co-doped UiO-66 nanoparticle with enhanced removal efficiency of tetracycline: simultaneous adsorption and photocatalysis, *Chem. Eng. J.* 353 (2018) 126–137.
- [48] S. He, B. Yin, H. Niu, Y. Cai, Targeted synthesis of visible-light-driven covalent organic framework photocatalyst via molecular design and precise construction, *Appl. Catal. B Environ.* 239 (2018) 147–153.

Ball Milling Synthesis of Covalent Organic Framework as a Highly Active Photocatalyst for Degradation of Organic Contaminants

Hongzhou Lv^{a,b,c}, Xiaoli Zhao^{a*}, Hongyun Niu^b, Sijing He^b, Zhi Tang^a, Fengchang Wu^a and John P. Giesy^d

^a State Key Laboratory of Environmental Criteria and Risk Assessment, Chinese Research Academy of Environmental Sciences, Beijing 100012, China

^b State Key Laboratory of Environmental Chemistry and Ecotoxicology, Research Center for Eco-Environmental Sciences, Chinese Academy of Sciences, Beijing 100085, China

^c College of Environment, Hohai University, Nanjing 210098, China

^d Department of Veterinary Biomedical Sciences and Toxicology Centre, University of Saskatchewan, Saskatoon, Saskatchewan, Canada

Supporting Information

Experimental Section.

Characterization methods.

Structure of prepared COFs were analysed by use of elemental analysis (EA3000 analyzer), Fourier transform-infrared (FT-IR) spectra (Thermo Nicolet NEXUS 670), powder x-ray diffraction analyses (PXRD, PANalytical X'Pert diffractometer) and x-ray photo-electron spectroscopy (XPS, Thermo Fisher ESCALAB 250Xi). Field-emission scanning electron microscopy (FE-SEM, Hitachi S-5500) and transmission electron microscopy (TEM, Hitachi H-7500) were applied to characterize particles. Thermal stability of TpMA was carried out using thermo-gravimetric analysis (TGA, Q5000 IR thermo-gravimetric analyzer). Specific surface areas of synthesized COFs were measured with Brunauer-Emmett-Teller (BET,

Quadrascorb SI surface area and pore size analyzer). Photo-electrochemical properties were collected by use of diffuse reflectance spectra (DRS, Hitachi U-3900 UV-vis spectrophotometer, BaSO₄ as reflectance standard), photoluminescence emission spectroscopy (PL, Hitachi F-7000 fluorescence spectrophotometer) and electro-chemical impedance spectroscopy (EIS, Chenhua CHI660E electrochemical analyzer).

Photocurrent responses were measured via a standard three-electrode system, by use of TpMA sample as well as platinum foil and Ag/AgCl (saturated KCl) as working electrode, counter electrode and reference electrode, respectively. Working electrodes were prepared by mixing 5 mg sample powder with 0.5 mL DMF and trace 5% Nafion, then dip coated on the conductive surface of indium tin oxide (ITO) glass and dried at 100 °C. 0.1 M sodium sulfate served as the electrolyte solution and source of the visible light is 300 W xenon lamp with a 420 nm cut-off filter. Photocurrent responds were obtained through switching the lamp on or off during the identical interval time.

Table S1 The content of C, N, O and H in TpMA using element analysis

element	Liquid-free route	Solvent-assisted route						Catalyst-assisted route	
	TpMA _{SEAF}	TpMA _{Si(1ml)}	TpMA _{Si(3ml)}	TpMA _{Sz(1ml)}	TpMA _{Sz(3ml)}	TpMA _{Si(1ml)}	TpMA _{Si(3ml)}	TpMA _{Cl(1ml)}	TpMA _{Cl(3ml)}
C	50.58%	51.67	51.70	50.59	50.77	51.74	51.64	51.34	50.90
N	28.34%	27.50	26.10	32.43	30.08	25.50	28.31	29.15	29.48
O	17.58	16.57	17.48	15.86	15.82	18.31	16.57	17.18	16.97
H	3.5	4.26	4.72	1.12	3.33	4.45	3.48	2.33	2.65

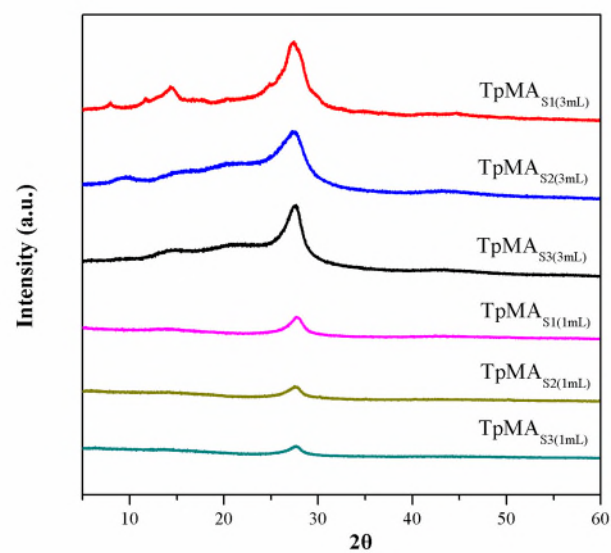


Fig. S1 PXRD of $\text{TpMA}_{\text{S}(1\text{mL})}$ and $\text{TpMA}_{\text{S}(3\text{mL})}$.

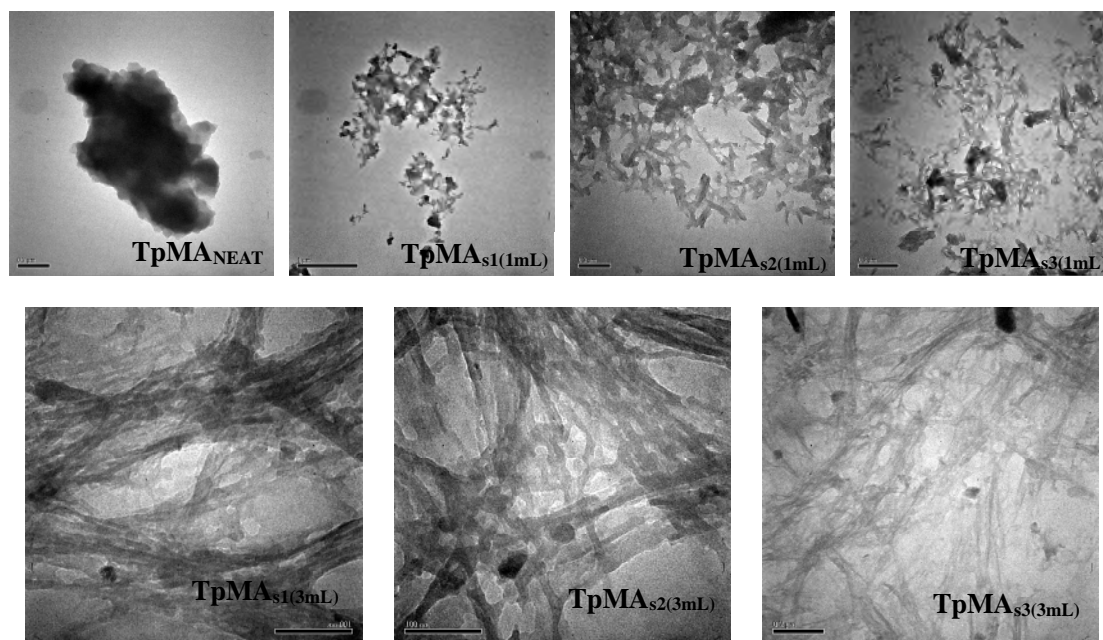


Fig. S2 TEM of $\text{TpMA}_{\text{NEAT}}$, $\text{TpMA}_{\text{S}(1\text{mL})}$ and $\text{TpMA}_{\text{S}(3\text{mL})}$.